ACS Catalysis

Research Article

pubs.acs.org/acscatalysis

Selective Electrochemical Reduction of Carbon Dioxide to Ethylene and Ethanol on Copper(I) Oxide Catalysts

Dan Ren, Yilin Deng, Albertus Denny Handoko, Chung Shou Chen, Souradip Malkhandi, and Boon Siang Yeo*

Department of Chemistry, Faculty of Science, National University of Singapore, 3 Science Drive 3, Singapore 117543

Supporting Information

ABSTRACT: The selective electroreduction of carbon dioxide to C_2 compounds (ethylene and ethanol) on copper(I) oxide films has been investigated at various electrochemical potentials. Aqueous 0.1 M $KHCO_3$ was used as electrolyte. A remarkable finding is that the faradic yields of ethylene and ethanol can be systematically tuned by changing the thickness of the deposited overlayers. Films 1.7−3.6 μm thick exhibited the best selectivity for these C_2 compounds at −0.99 V vs RHE, with faradic efficiencies (FE) of 34−39% for ethylene and 9−16% for ethanol. Less than 1% methane was formed. A high C_2H_4/CH_4 products' ratio of up to ∼100 could be achieved. Scanning electron microscopy, X-ray diffraction, and in situ Raman spectroscopy revealed that the Cu_2O films reduced rapidly and remained as metallic Cu^0 particles during the CO_2 reduction. The selectivity trends exhibited by the catalysts during CO_2 reduction in phosphate buffer, and $KHCO_3$ electrolytes suggest that an increase in local pH at the surface of the electrode is not the only factor in enhancing the formation of C_2 products. An optimized surface population of edges and steps on the catalyst is also necessary to facilitate the dissociation of CO_2 and the dimerization of the pertinent CH_xO intermediates to ethylene and ethanol.

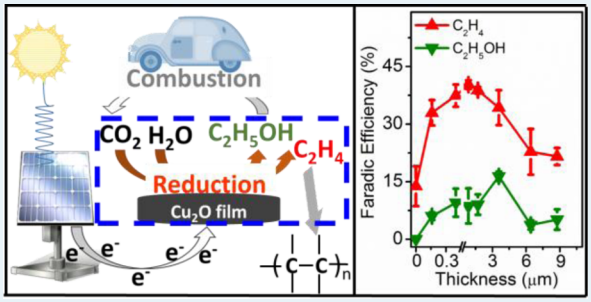

KEYWORDS: *ethylene, ethanol, selectivity, CO_2 reduction, Cu_2O, electrocatalysis*

1. INTRODUCTION

The reduction of carbon dioxide (CO_2) to hydrocarbons and alcohols has the potential to generate a sustainable supply of valuable feedstocks for our chemical industries and fuels to meet our energy needs.[1−9] Alongside with carbon sequestration, it is also an effective way to mitigate anthropogenic CO_2 emissions. Among the CO_2 reduction products, ethylene (C_2H_4) and ethanol (C_2H_5OH) have higher energy densities and commercial value than their C_1 counterparts such as methane (CH_4).[10−13] Ethylene and ethanol can be formed on the surface of a catalyst via the following half-reactions.[2,14,15]

$$2CO_2 + 8H_2O + 12e^- \rightarrow C_2H_4 + 12OH^-$$

$$2CO_2 + 9H_2O + 12e^- \rightarrow C_2H_5OH + 12OH^-$$

It is believed that CO_2 is first reduced through multiple proton−electron transfers to surface-bound $*CH_xO$ (x = 0, 1, 2). These moieties then undergo intermolecular C−C bond formation to yield $*C_2H_xO_2$ (x = 0−4), which are further reduced to ethylene and ethanol.[16] To date, copper-based materials are the most promising electrocatalysts for this reaction, albeit still rather unselective.[17−21] Considerable and urgent efforts have therefore been devoted to tuning the structure and composition of copper catalysts with the aim of optimizing their CO_2-to-C_2 selectivity.[19−25]

The type of products formed during CO_2 electroreduction is significantly impacted by the electrolytes used, potentials applied, and the morphology and surface geometry of the copper surfaces (Table 1). On polycrystalline Cu surfaces poised at −5 mA/cm^2 in 0.1 M $KHCO_3$, the faradic efficiencies (FE) for the production of C_2 compounds (ethylene and ethanol) and methane are ∼37 and ∼29%, respectively.[17] The dismal selectivity can be attributed to the heterogeneity of catalytic sites present on the polycrystalline Cu plane. This can be ameliorated by tuning the potentials of the working electrode, although enhancements have not been significant.[18,26] More improvements were found when CO_2 reduction was performed on single crystal Cu(100) surfaces and even more so on cleaved Cu(100) substrates with high-indexed planes.[27] In particular, ethylene and ethanol could be produced from the electroreduction of CO_2 with a total FE of ∼57% on the Cu(S)-[4(100) × (111)] surface. The square arrangement of the Cu atoms in the (100) terraces and presence of atomic steps have been proposed to favor C−C bond coupling between the CH_xO intermediates to give C_2 compounds;[2] however, the use of single crystal surfaces is not practical for scaling up catalytic processes for the chemical industries. Recently, our group discovered that copper mesocrystals formed by the in situ reduction of a CuCl film were active toward the reduction of CO_2 to C_2H_4 with a C_2H_4/CH_4

Received: December 31, 2014
Revised: March 16, 2015
Published: March 31, 2015

DOI: 10.1021/cs502128q
ACS Catal. 2015, 5, 2814−2821

Table 1. An Overview of Faradic Efficiencies of Products (%) Obtained from CO_2 Reduction on Various Copper Catalysts[a]

			faradic efficiencies (%)							
catalyst	electrolyte	experimental conditions	C_2H_4	C_2H_5OH	C_2H_6	CO	CH_4	formic acid	other C_{2+}	C_2H_4/CH_4
polycrystalline Cu[17]	0.1 M $KHCO_3$	−5 mA/cm^2	30.1	6.9	N.R.	2.0	29.4	9.7	3.0	1.0
polycrystalline Cu[18]	0.1 M $KHCO_3$	−1.05 V vs RHE	26.0	9.8	N.R.	1.1	24.4	2.1	4.8	1.1
Cu(100)[27]	0.1 M $KHCO_3$	−5 mA/cm^2	40.4	9.7	N.R.	0.9	30.4	3.0	7.7	1.3
Cu(S)-[4(100) × (111)][27]	0.1 M $KHCO_3$	−5 mA/cm^2	50.0	7.4	N.R.	1.1	5.0	4.6	14.1	10
Cu mesocrystals[26]	0.1 M $KHCO_3$	−0.99 V vs RHE	27.2	N.R.	N.R.	0.55	1.47	4.3	N.R.	18
Cu-halide confined mesh[23]	3 M KX (X = Br, I, or Cl)	−2.4 V vs Ag/AgCl	60.5−79.5	1.6−1.9	0.8−2.8	1.8−2.8	4.3−6.6	0.1−0.7	0.1−0.6	9−17
electrodeposited Cu_2O[21]	0.1 M $KHCO_3$	−1.1 V vs RHE	12−33	N.R.	0−9	1−3	0−4	22	N.R.	8−12
electrodeposited Cu_2O[28]	0.5 M $KHCO_3$	−1.82 V vs Ag/AgCl	26	N.R.	N.R.	6	1	8	N.R.	26
Cu nanoparticles[19]	0.1 M $KClO_4$	−1.1 V vs RHE	36	N.R.	∼1	34	1	N.R.	N.R.	36

[a] C_{2+} contains all other compounds with ≥2 carbon atoms. N.R.: not reported.

product ratio of 18.[26] High-resolution transmission electron microscopy revealed the presence of numerous (100) facets and atomic steps on the Cu mesocrystals, which we assigned as the catalytically active sites.

Cu^I-halide-coated electrodes, CuO, electrodeposited Cu nanoparticles and reduced Cu_2O films are also catalytically selective in reducing CO_2 to C_2 compounds.[19,21,23,26,28,29] The Cu_2O films were formed by electrodepositing Cu ions on metal substrates or thermal heating of Cu metal films.[20,21,30] These films were found to have nanoparticulate morphologies. Kanan and co-workers demonstrated that reduced Cu_2O films could reduce CO to C_2H_5OH with a FE of 43%.[24] Grain boundaries on the surfaces of these films have been postulated to be the driving forces for the C_2 product selectivity.[19,24] Their role could be to stabilize and facilitate the dimerization of the pertinent C_1 reaction intermediates. Recently, Kas et al. showed that C_2H_4 could be produced with a FE of up to 33% on thick Cu_2O films, but no C_2H_5OH could be detected.[21,31] When the electrolyte concentration was decreased, the C_2H_4/CH_4 ratio increased; thus, the selectivity is believed to be caused by a higher local pH at the surface of the electrode.[32]

Inspired by these studies, we have investigated the electrochemical reduction of CO_2 on Cu_2O films in aqueous 0.1 M $KHCO_3$ electrolytes. Cu_2O films of different thicknesses were formed by galvanostatic deposition. In addition to ex situ scanning electron microscopy and X-ray diffraction, in situ Raman spectroscopy was used for the first time, to probe changes in the chemical and structural composition of the Cu_2O films during the CO_2 reduction. Ethylene and ethanol were substantially formed on these films. Methane production was practically suppressed on the thicker films. The factors underlying the changes in selectivity are discussed in terms of morphology of the catalysts and effects of local pH at the surface of the electrodes.

2. EXPERIMENTAL SECTION

2.1. Catalyst Preparation. Flat Cu discs (⌀=10 mm, 99.99%, Goodfellow) served as substrates for all the catalysts. They were first polished to a mirror-like finish using SiC paper (grit 1200, Struers) and diamond slurries (Diapro 9 and 3 μm, Struers). Cu_2O layers were then galvanostatically deposited onto these Cu discs (exposed geometric surface area: 0.385 cm^2) from a copper lactate solution (Supporting Information S1).[33] Cu_2O films of different thicknesses were obtained by varying the deposition time between 1 and 60 min. Seven Cu_2O films with varying thicknesses were prepared. Electropolished Cu surfaces were prepared by electropolishing the copper discs at +260 mA/cm^2 for 60 s in 85% phosphoric acid (Sigma-Aldrich), followed by rinsing with ultrapure water (Type 1, Barnstead, Thermo Scientific).[17]

2.2. Characterization of Copper Catalysts. The thickness and surface morphology of the Cu_2O films were imaged using scanning electron microscopy (JEOL JSM-6710F, 5 keV) (Supporting Information S1). X-ray diffraction (Bruker D8 Discover with GADDS, 40 keV, 40 mA) was used to analyze the chemical composition of the films. The films were removed from the Cu substrates for XRD analysis by using a sharp blade. The XRD patterns of Cu_2O and Cu^0 were identified by comparisons with their respective standards, PDF 00-003-0892 and PDF 00-001-1242.

In situ Raman spectroscopy was performed using a confocal Raman microscope (modular system, Horiba Jobin Yvon) in an epi-illumination mode (top-down). A schematic diagram of the setup is provided in Supporting Information S2. The excitation source was a He−Ne laser with 633 nm wavelength (CVI Melles Griot). A water immersion objective lens (LUMFL, Olympus, 60×, numerical aperture: 1.10) covered with a 0.013 mm thin Teflon film (American Durafilm) was used for focusing and collecting the incident and scattered laser light.[34] The backscattered light was filtered by a 633 nm edge filter and directed into a spectrograph (iHR320)/charge-coupled device detector (Synapse CCD). The acquisition time for each spectrum was 5 s. The electrochemical cell was based on a round Teflon dish, with the working electrode firmly mounted at its base.[34] Counter and reference electrode were inserted into the cell via port holes.

The electrochemically active surface area (ECSA) of the catalysts was measured by the double-layer capacitance measurement method (Supporting Information S1).[30]

DOI: 10.1021/cs502128q
ACS Catal. 2015, 5, 2814−2821

2.3. Electrochemical Setup, Identification and Quantification of CO_2 Reduction Products. A custom-built, gastight Teflon electrochemical cell based on the design of Kuhl et al. was used (Figure 1).[18,26] The cathodic and anodic

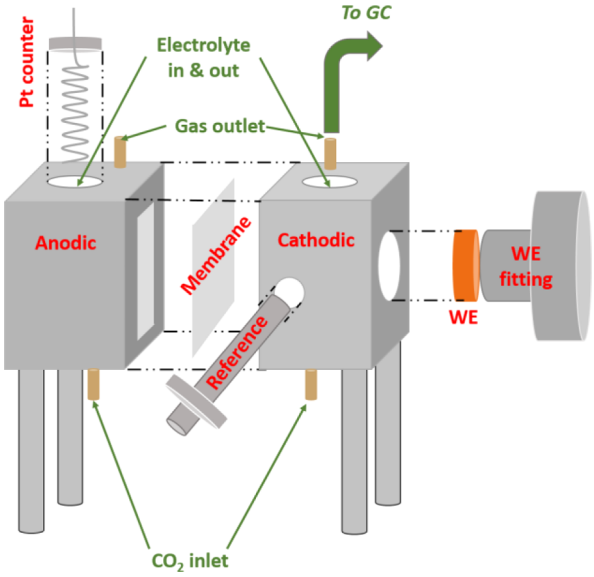

Figure 1. Schematic diagram of the electrochemical cell used for CO_2 electroreduction. WE: working electrode.

compartments, separated by an anion-exchange membrane (Selemion AMV, AGC Asahi Glass), were filled with 10 and 8 cm^3 of electrolyte separately. The volume of the headspace in the cathodic compartment was 2 cm^3. A coiled platinum wire and Ag/AgCl (Saturated KCl, Pine) served as counter and reference electrodes, respectively. The calibration of the reference electrode was checked against a reversible hydrogen electrode (RHE, HydroFlex, Gaskatel).

Aqueous 0.1 M $KHCO_3$ (Merck, 99.7%) and phosphate buffer (0.1 M K_2HPO_4, Sigma-Aldrich, >99.0% and 0.1 M KH_2PO_4, Sigma-Aldrich, >99.0%) were used as electrolytes. The latter was purified by pre-electrolysis under N_2 gas for 20 h.[17,35] Prior to CO_2 reduction, the electrolytes were saturated with CO_2 gas (99.999%, Linde Gas) for 10 min. During the experiment, CO_2 was bubbled into the electrolyte at a flow rate of 20 sccm. The electrolyte was stirred using a Teflon-coated magnetic stirrer bar at 1500 rotations per minute (rpm) to enhance mass flow of CO_2 to the working electrode.

A potentiostat (Gamry Reference 600) was used for controlling and measuring the potentials/currents. Compensation for *iR* drop was made using the current interrupt mode. All the measured potentials in this work are cited with respect to the RHE using the following conversion: E_{RHE} (V) = $E_{Ag/AgCl}$ (V) + 0.197 V + (0.059 V × pH). The pH values of the electrolytes are listed in Supporting Information S3. Unless otherwise stated, the current density values reported in this work were normalized to the geometric surface area.

The experimental protocol for identifying and quantifying the products formed during CO_2 electroreduction has been reported in our previous publication.[26] The headspace of the cathodic compartment was continuously purged by the incoming CO_2 (with reduction products) into the sampling loops of the gas chromatograph (GC, Agilent, 7890A). Gas aliquots were analyzed after 3, 14, 26, 37, 48, and 59 min of chronoamperometry. To ensure that the reported data is from a system under equilibrium condition, only the average of the third to the sixth GC measurements was used in the data analysis (Supporting Information S5). The liquid products in the catholyte were analyzed at the end of the chronoamperometry using ^1H nuclear magnetic resonance spectroscopy (NMR, Avance 300, Bruker) (Supporting Information S4).[18,26] The product yields were expressed as faradic efficiencies (Supporting Information S5). Each data point is an average of the measurements collected from at least three separate NMR or GC experiments. Each prepared catalyst was used only once for CO_2 reduction at a chosen potential. Potentials between −0.59 and −1.19 V were applied.

3. RESULTS AND DISCUSSIONS

3.1. Characterization of Copper Catalysts. The as-prepared catalysts, which consist of an electropolished Cu electrode and seven Cu_2O films, were characterized by scanning electron microscopy, X-ray diffraction, and in situ Raman spectroscopy (Figure 2). The thicknesses of the Cu_2O films were estimated by SEM imaging of their cross sections, and were found to be 0.2, 0.4, 0.9, 1.7, 3.6, 6.4, and 8.8 μm thick (Supporting Information S1). Representative SEM images of these electrodes are shown in Figure 2A−D. As the deposition time of Cu_2O lengthened, the appearance of the pristine Cu disc changed from flat and featureless to particulate. The size of the particles increased systematically with thickness of the deposited Cu_2O layer, with ∼100-nm-sized nanoparticles for the thinnest 0.2 μm film and ∼2−3 μm-sized polyhedron particles with many well-defined edges for the 8.8 μm film. X-ray diffraction of the bulk films demonstrated that they are Cu_2O (Figure 2I).

Reduction of CO_2 (4200 s) was performed using these catalysts. At the end of the reaction, their surfaces were again examined by SEM. Images of electrodes reduced at a representative potential of −0.99 V are shown in Figures 2E−H. The surface of the electropolished Cu remained smooth (Figure 2E). The reduced 0.2 μm film consisted of nanoparticles ∼100 nm in size (Figure 2F), and large polyhedron particles were observed on the thicker films (Figures 2G,H, Supporting Information S6). These thick films have a rough surface morphology, as indicated by the numerous small nanoparticles on their surface and their high surface roughness factors (Supporting Information S1). Time-resolved ex situ SEM images show that cracks observed on the thicker films appear early on during the CO_2 reduction process (Figure 2G,H, Supporting Information S6). These could be due to relief of strains caused by volume changes in the films during their reduction.[36] Indeed, only Cu^0 reflexions were observed in the X-ray diffractograms of the reduced films, which demonstrates that the bulk of the Cu_2O films had reduced to metallic Cu during the course of the CO_2 reduction (Figure 2J).

We also employed in situ Raman spectroscopy to probe the surface of the Cu_2O films in real time during CO_2 reduction. Raman spectra of a representative 1.7 μm Cu_2O film held at −0.99 V are presented in Figure 2K. Cu_2O, as evidenced by its vibrational fingerprints at 147, 218, 526, and 624 cm^{-1}, was detected at the start of the CO_2 reduction (at 0 s).[37] These peaks were attenuated after 30 s, which demonstrate the rapid reduction of the top layers of the Cu_2O film. Two bands centered at 365 and 502 cm^{-1} concurrently appeared. These can be attributed to the Cu−O vibrations of intermediately reduced Cu oxides.[37] From 200 s onward, no peaks could be observed in the Raman spectrum. This signifies that the surface

DOI: 10.1021/cs502128q
ACS Catal. 2015, 5, 2814−2821

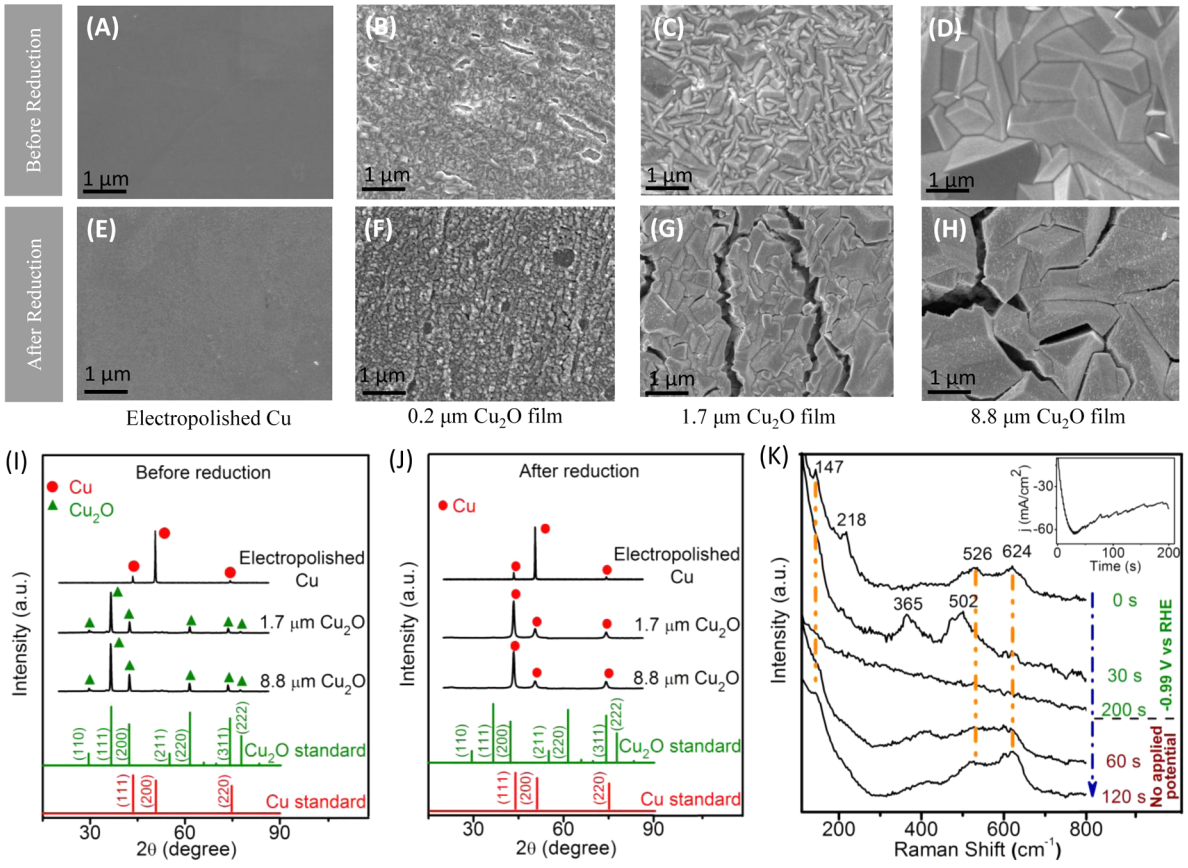

Figure 2. SEM images of Cu catalysts before CO_2 reduction: (A) electropolished Cu; (B) 0.2 μm, (C) 1.7 μm, and (D) 8.8 μm Cu_2O films deposited on Cu disc. SEM images of Cu catalysts after CO_2 reduction at −0.99 V: (E) electropolished Cu; (F) 0.2 μm, (G) 1.7 μm, and (H) 8.8 μm Cu_2O films deposited on Cu disc. XRD of Cu catalysts (I) before and (J) after CO_2 reduction. The standard patterns (vertical line) are also included for comparison (PDF 00-003-0892 for Cu_2O and PDF 00-001-1242 for Cu). (K) In situ Raman spectra and corresponding chronoamperogram (inset) of 1.7 μm film at −0.99 V in 0.1 M $KHCO_3$.

of the Cu_2O films has been reduced to metallic copper during CO_2 reduction. After the cathodic potential was removed, the surface reoxidized in tens of seconds to Cu_2O, as shown by the appearance of its Raman bands at 147, 520, and 624 cm^{-1} (Figure 2K). Similar observations were made (Cu_2O reduced to Cu^0 rapidly) when other cathodic potentials were applied (Supporting Information S2). Because of the insufficient limits of detection afforded by our spectrometer, no Raman signals belonging to adsorbed CO_2 or its reduced species (whose surface population is likely to be ≤1 monolayer) could be discerned.

On the basis of evidence from ex situ XRD and elemental depth profiling using Auger electron spectroscopy, the oxidized state of a Cu_2O film has been proposed to be partially conserved during CO_2 reduction.[28] Cu^+ ions were thus suggested to be catalytic active for reducing CO_2 to C_2 compounds. We have shown, however, that the surface of a Cu_2O film reduces and remains as metallic Cu particles during electrochemical CO_2 reduction. This finding is consistent with predictions from the Pourbaix diagram of the copper-water system.[38] We thus believe that Cu^0 particles are the catalytic active species for reducing CO_2. To the best of our knowledge, this is the first in situ spectroscopic study of copper oxide films during CO_2 reduction.

3.2. Electrochemical Reduction of CO_2 to C_2 Products.

CO_2 reduction was performed using the Cu catalysts at fixed potentials between −0.59 and −1.19 V. Figure 3 shows

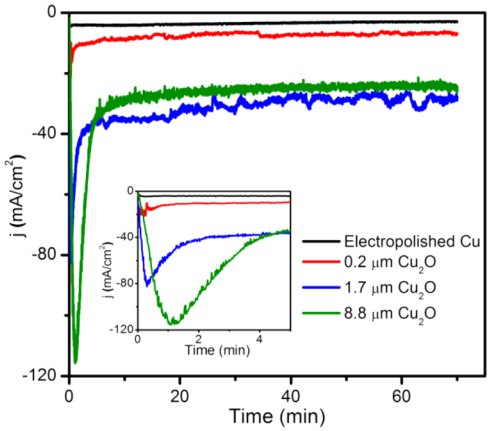

Figure 3. CO_2 reduction current as a function of time for four representative Cu catalysts. The inset is a zoomed-in view of the curves in the first 5 min. Potential applied: −0.99 V. Electrolyte: 0.1 M $KHCO_3$.

representative chronoamperometry curves taken at −0.99 V for electropolished Cu as well as 0.2-, 1.7-, and 8.8-μm-thick Cu_2O catalysts. Reduction peaks were observed in all the chronoamperometry curves of the Cu_2O catalysts during the initial phase of the CO_2 reduction process. This feature, in agreement with the XRD and Raman spectroscopy results presented in Section 3.1, can be attributed to the reduction of

DOI: 10.1021/cs502128q
ACS Catal. 2015, 5, 2814−2821

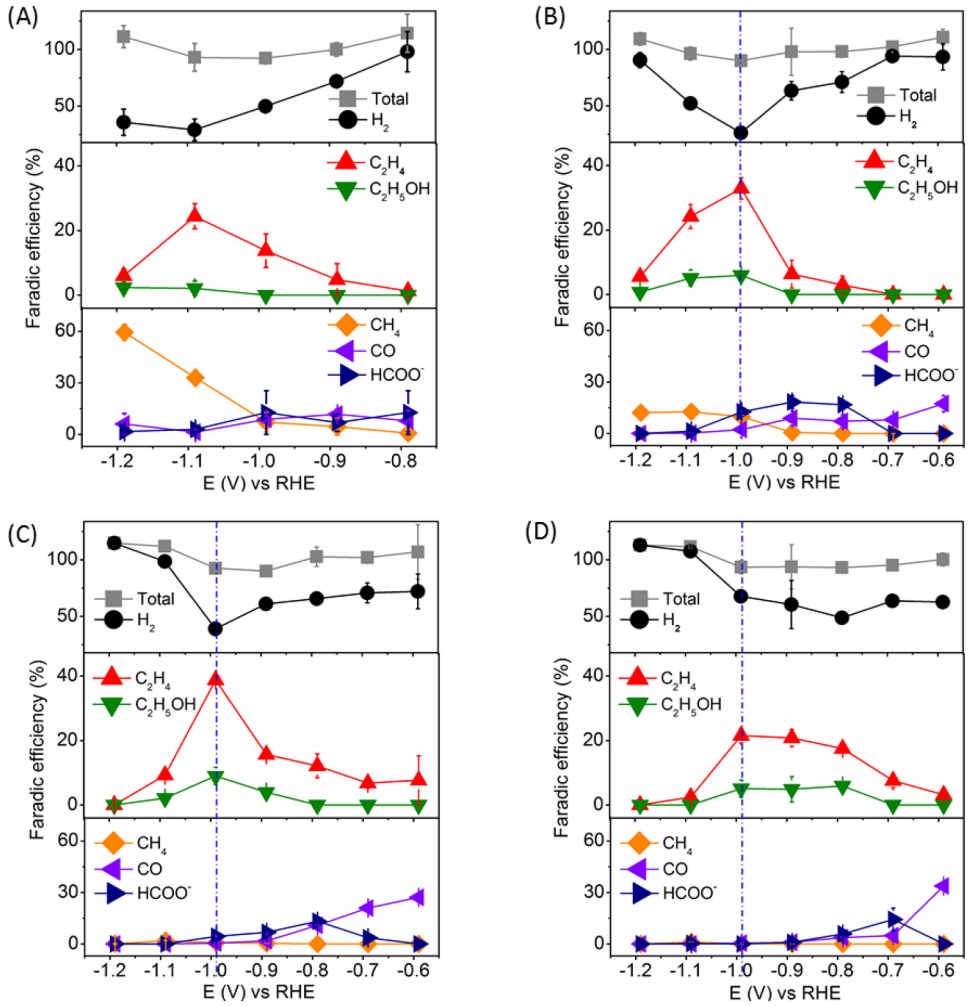

Figure 4. Faradic efficiencies for CO_2 electroreduction products as a function of potential. (A) Electropolished Cu; (B) 0.2, (C) 1.7, and (D) 8.8 μm Cu_2O film deposited on Cu disc. Electrolyte: 0.1 M $KHCO_3$.

Table 2. Faradic Efficiencies of Products (%) Obtained from CO_2 Reduction on Electropolished Cu and Cu_2O Catalysts[a]

		faradic efficiencies (%)							
catalyst	j (mA/cm^2)	CO	CH_4	C_2H_4	C_2H_5OH	C_2H_6	$HCOO^-$	H_2	total
polished Cu	−3	8.82	7.14	13.79	N.D.	N.D.	12.76	49.78	92.29
0.2 μm film	−14	2.25	9.85	32.92	6.00	N.D.	12.67	26.21	89.90
0.4 μm film	−20	1.54	6.93	37.40	9.50	N.D.	2.48	31.01	88.86
0.9 μm film	−25	0.66	2.48	40.25	8.66	0.04	8.34	28.60	89.03
1.7 μm film	−30	0.49	0.73	38.79	9.01	0.08	4.45	38.98	92.53
3.6 μm film	−35	0.43	0.32	34.26	16.37	0.15	3.94	38.87	94.34
6.4 μm film	−30	0.37	0.18	22.76	3.71	0.10	1.25	63.80	92.17
8.8 μm film	−29	0.52	0.15	21.55	5.10	0.15	N.D.	67.67	95.14

[a]Reduction carried out in 0.1 M $KHCO_3$ at −0.99 V. N.D.: not detectable.

Cu_2O to Cu^0. When the steady state currents were compared, the electrodes deposited with Cu_2O films exhibited higher current densities compared with the electropolished Cu. This can be attributed to the formers' larger surface roughness and, hence, electrochemically active surface areas (Supporting Information S1). A modest decrease in the currents of the catalysts could be observed during the reduction reaction. This could be due to the buildup of gas bubbles at the interface of the electrode, which blocks available catalytic sites. An increase in the temperature of the electrolyte during the reaction could also result in poorer solubility of CO_2 in the electrolyte and, hence, cause a decrease in the current density.[18]

The faradic efficiency for each CO_2 reduction product as a function of potential is presented in Figure 4. Carbon monoxide, methane, formate, ethylene, ethanol, and trace amounts of ethane (0.1%) were found (Supporting Information S5). H_2 was a product of the competitive hydrogen evolution reaction (HER).[14] The faradic efficiencies of the products in all experiments amount to 89−114%, which showed that all the major products have been accounted for.[17] The product distribution trend exhibited by the electropolished Cu electrode

DOI: 10.1021/cs502128q
ACS Catal. 2015, 5, 2814−2821

Table 3. Faradic Efficiencies of Products (%) Obtained from CO_2 Reduction on Electropolished Cu and Cu_2O Catalysts[a]

		faradic efficiencies (%)							
catalyst	j (mA/cm^2)	CO	CH_4	C_2H_4	C_2H_5OH	C_2H_6	$HCOO^-$	H_2	total
polished Cu	−14	0.02	0.27	0.03	N.D.	0.01	5.60	95.25	101.18
0.2 μm film	−26	0.40	9.49	8.09	7.90	0.29	8.53	61.20	95.90
1.7 μm film	−48	0.20	1.11	16.12	5.11	0.58	2.15	69.27	94.54
8.8 μm film	−52	0.28	0.28	7.00	2.33	0.09	1.16	97.21	108.35

[a]Reduction carried out in phosphate buffer saturated with CO_2 (pH = 6.73) at −0.99 V. N.D.: not detectable.

toward CO_2 reduction is consistent with previous studies (Figure 4A);[18,26] however, the FE of CH_4 at −1.19 V is 59%, which is significantly higher than what was achieved in our earlier report.[26] This could be attributed to the smaller volume (10 cm^3) of catholyte used in the present electrochemical cell, which enhances the concentration of dissolved CO_2. When CO_2 reduction is performed using the Cu_2O films, CH_4 production dramatically decreases, especially on the thicker films. For films thicker than 1.7 μm, the FE of CH_4 is <2%, regardless of the applied potential. The Cu_2O films exhibited generally better selectivity for CO_2 reduction to C_2 compounds.

We observed that the selectivity of Cu_2O catalysts toward C_2 compounds was optimized at −0.99 V. A detailed analysis of the compounds formed at this potential is thus presented in Table 2. A remarkable finding is that the FEs of ethylene and ethanol change systematically (a parabolic trend) as a function of thickness of the Cu_2O films. The FE of ethylene and ethanol could be tuned between 22−40%, and 4−16%, respectively. In contrast, the FE of CH_4 decreased rapidly to <1% as the thickness of the films increased.

The 1.7−3.6-μm-thick Cu_2O films exhibited optimum selectivity toward the formation of C_2 products. FEs of 34−39% and 9−16% for ethylene and ethanol were respectively formed using these films; the FE of methane was 0.3−0.7%. The FE of ethanol in this work is notably high (Table 1).[19,21,27] The selectivity of our Cu catalysts can also be assessed by its C_2H_4/CH_4 ratio, which is a useful figure of merit for assessing the intrinsic C_2 selectivity of a material.[21,27,39] Here, the 3.6-μm-thick films exhibit a C_2H_4/CH_4 of up to ∼100, which compares very favorably with other C_2-selective catalysts, including Cu_2O films (Table 1).[19,21,26,27]

It is significant that C_2H_4 and C_2H_5OH were formed at similar potential regimes, and that the FE of C_2H_4 is always higher than that of C_2H_5OH (Figure 4 and Table 2). These observations demonstrate that these two molecules originate from a common reaction intermediate.[18] On the basis of density functional theory (DFT) calculations, *CH_2CHO has been proposed to be the key intermediate.[40] The higher FE of C_2H_4 compared with C_2H_5OH has been attributed to a more energetically favorable hydrogenation of *CH_2CHO to C_2H_4. Another notable observation is that our reduced Cu_2O films exhibited lower overpotentials by 0.1−0.2 V for the optimization of C_2 selectivity compared with other similarly synthesized Cu_2O films.[28]

To ascertain if the selectivity differences result from changes in CO_2 reduction activity or H^+ reduction activity, we normalized the partial current density of the products with the ECSA of the catalysts (Supporting Information S7). The partial current densities of C_2H_4 and H_2 exhibited by the 1.7−3.6 μm films were ∼4 and ∼1.3 times larger, respectively, than those on the electropolished Cu. The partial current density for CH_4 was substantially decreased. We thus attribute the selectivity differences to mainly changes in the CO_2 reduction activity of the catalysts.

3.3. Effects of Local pH on C_2 Products Selectivity. We assess the effects of local pH on the selectivity of the reduced Cu_2O electrocatalysts by examining the data in Table 2. The geometric current densities and faradic efficiency of H_2 increased continuously with the thickness of the Cu_2O films, which agrees with the work by Kas et al.[21] This would result in a higher local pH at the surface of the electrode, which may explain the observed suppression of CH_4 production and increased selectivity toward C_2H_4; however, the FE for C_2H_4 decreased on the 6.4 and 8.8 μm films. This suggests that the effects of local pH may not be the sole factor in dictating the selectivity; morphological factors could also contribute to the phenomenon. Mass transport limitations of CO_2 to these electrodes that have high electrochemically active surface areas may also result in a lower C_2H_4 production. It is difficult, though, to estimate the extent of this effect in relation to CO_2 reduction as the electrolyte is vigorously stirred during the experiment.

CO_2 reduction was also performed on the 0.2-, 1.7-, and 8.8-μm-thick films in phosphate buffer electrolytes (Table 3). Buffers mitigate increases in local pH at the surface of the electrode during CO_2 reduction and are expected to favor the formation of CH_4.[17] Although the FEs for C_2H_4 decreases to <16%, which agrees with previous studies that C_2H_4 formation is disfavored in phosphate buffers, CH_4 formation does not increase.[14,17] This trend argues against changes in local pH as the sole factor for the enhanced selectivity of the Cu_2O films toward C_2 compounds. The local structure of our catalysts is likely to be of significant importance.

No gaseous or liquid products could be detected from the cathodic compartment in the absence of applied potentials on the working electrode (Supporting Information S4). Thus, all the products observed in this work must originate from the electrocatalytic reduction of CO_2 on the Cu catalysts.

3.4. Enhanced Intermolecular C−C Coupling of C_1 Moieties on Copper Surfaces To Give C_2 Products. A mechanistic model for the electrochemical reduction of CO_2 to ethylene and ethanol is shown in Figure 5. First steps involve proton and electron transfer to give a *COOH surface moiety, which can then hydrogenate to give H_2O and adsorbed *CO.[41,42] Moderately adsorbed *CO species can further hydrogenate to CH_4, or dimerize/hydrogenate to *$C_2H_xO_2$.[18,32] This intermediate can then be subsequently reduced to either ethylene or ethanol. Quantum chemical simulations suggest that the intermolecular C−C coupling process is more kinetically favorable when the immediate reactants are *CHO or *CH_2O, rather than *CO.[16] We have also demonstrated in this work using SEM, XRD, and in situ Raman spectroscopy that the catalytically active sites responsible for the selective formation of C_2 compounds are Cu^0 particles. Both local pH effects and morphological factors

DOI: 10.1021/cs502128q
ACS Catal. 2015, 5, 2814−2821

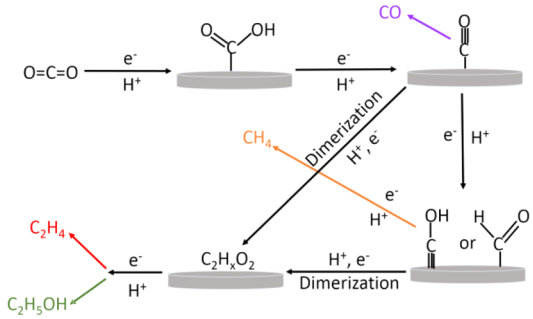

Figure 5. Proposed mechanism for the electroreduction of CO_2 to ethylene and ethanol on copper surfaces. (H_2O molecules are not drawn).

are likely to play significant roles in driving the selectivity of the CO_2 reduction reaction toward C_2 products.

C_2 selectivity is optimized with the 1.7−3.6-μm-thick films, which consisted of 0.5−1-μm-sized Cu polyhedrons. During CO_2 reduction, stepped surfaces with edges and terraces are likely to be formed as the Cu_2O film reduces to Cu.[22,24,26] Although it is difficult to quantify their surface population in our reduced Cu_2O films, we propose that an optimum combination of these features must be necessary to dissociate CO_2 and to optimize the chemisorption energies of the CH_xO intermediates. A critical role of the edges (with undercoordinated Cu atoms) is to promote the buildup of a large coverage of CH_xO reactive intermediates, to facilitate their dimerization. This is in agreement with predictions by density functional theory calculations and with a temperature-programmed desorption study showing that CO does adsorb more strongly on Cu steps and edges, as compared with Cu terraces.[16,19,43] We highlight here that Hori et al. had previously demonstrated that an optimization of step density on Cu(100) surfaces is necessary for the enhanced formation of C_2 compounds.[27,39] When either an excessive number of steps or too few steps are incorporated into a Cu(100) surface, C_2 selectivity decreases.

As the thickness of the Cu_2O film increases to 6.4−8.8 μm, production of both C_1 and C_2 compounds decreases while hydrogen evolution becomes more efficient (Table 2). This can be attributed to a larger surface population of Cu atoms with low coordination numbers (as suggested by the large roughness factors of these films). These undercoordinated atoms are expected to bind to atomic H more strongly as compared with Cu atoms on a planar surface. Because Cu lies on the right-hand side of the volcano curve for HER, an increase in its chemisorption strength toward H should result in the enhancement of HER compared with CO_2 reduction.[44,45] Similar observations have also been made on SnO_x films, where H_2 evolution increased continuously as the SnO_x films became thicker.[46] Mass transport limitations of CO_2 to the electrode may also lead to a more favorable catalysis of hydrogen evolution.

The faradic efficiencies for both methane and CO production are remarkably suppressed to <1% on the thicker (1.7−8.8 μm) films at −0.99 V. This could not be achieved on Cu single crystal electrodes, Cu mesocrystals, Cu halides, etc.[23,26,27] It is also significant that CH_4 suppression on a bulk Cu electrode could not be replicated by increasing the local pH at its surface by using nonbuffer electrolytes or lowering the concentrations of the $KHCO_3$ electrolyte.[17,32] This suggests that the selectivity of the films (shown in this work) toward C_2 products can be more adequately explained by the effects of local pH and morphological factors.

4. CONCLUSION

In summary, we have investigated the electroreduction of CO_2 on electrodeposited Cu_2O films at different potentials. The faradic yields for C_2 products can be systematically tuned by varying the thicknesses of the Cu_2O overlayers. The 1.7−3.6-μm-thick films exhibited the most efficient C−C bond formation to give ethylene and ethanol with faradic efficiencies 34−39 and 9−16%, respectively. The formation of methane was significantly suppressed (FE <1%). Thus, an unprecedentedly high C_2H_4/CH_4 products' ratio of up to ∼100 was achieved.

Materials analysis revealed that the highly selective catalyst film is metallic Cu in the form of 0.5−1-μm-sized polyhedron particles. Control experiments with phosphate buffer electrolytes suggest that variation in local pH at the surface of the electrode is not the only factor in influencing the product selectivity. The higher selectivity of the films toward C_2 compounds could also be attributed to their optimized density of steps and edges, a morphology widely believed to be essential for the formation of C_2 compounds from CO_2 reduction. More experimental and theoretical work is needed to understand the influence of steps and edges and how they impact the production of ethylene, ethanol, methane, and hydrogen. This work demonstrates that the careful design of the morphology of reduced Cu_2O films can significantly enhance its selectivity toward C_2 compounds and edges us closer to the engineering of an efficient, environmentally friendly and earth-abundant CO_2 reduction electrocatalyst.

■ ASSOCIATED CONTENT

Supporting Information

The following file is available free of charge on the ACS Publications website at DOI: 10.1021/cs502128q.

Experimental procedures, characterization of catalysts, Raman spectroscopy system and data, pH of electrolytes, NMR data, calculation of faradic efficiencies of products and SEM figures

■ AUTHOR INFORMATION

Corresponding Author

*Phone: +65 6516 2836. Fax: +65 6779 1691. E-mail: chmyeos@nus.edu.sg.

Notes

The authors declare no competing financial interest.

■ ACKNOWLEDGMENTS

This work is supported by a start-up grant (R143-000-515-133) from the National University of Singapore.

■ REFERENCES

(1) Whipple, D. T.; Kenis, P. J. A. *J. Phys. Chem. Lett.* **2010**, *1*, 3451−3458.
(2) Gattrell, M.; Gupta, N.; Co, A. *J. Electroanal. Chem.* **2006**, *594*, 1−19.
(3) Centi, G.; Perathoner, S. *Catal. Today* **2009**, *148*, 191−205.
(4) Kuhl, K. P.; Hatsukade, T.; Cave, E. R.; Abram, D. N.; Kibsgaard, J.; Jaramillo, T. F. *J. Am. Chem. Soc.* **2014**, *136*, 14107−14113.
(5) Lu, Q.; Rosen, J.; Jiao, F. *ChemCatChem* **2014**, *7*, 38−47.

DOI: 10.1021/cs502128q
ACS Catal. 2015, 5, 2814−2821

(6) Reske, R.; Mistry, H.; Behafarid, F.; Roldan Cuenya, B.; Strasser, P. *J. Am. Chem. Soc.* **2014**, *136*, 6978−6986.
(7) Baturina, O. A.; Lu, Q.; Padilla, M. A.; Xin, L.; Li, W.; Serov, A.; Artyushkova, K.; Atanassov, P.; Xu, F.; Epshteyn, A.; Brintlinger, T.; Schuette, M.; Collins, G. E. *ACS Catal.* **2014**, *4*, 3682−3695.
(8) Sen, S.; Liu, D.; Palmore, G. T. R. *ACS Catal.* **2014**, *4*, 3091−3095.
(9) Ogura, K. *J. CO_2 Util.* **2013**, *1*, 43−49.
(10) Farrell, A. E.; Plevin, R. J.; Turner, B. T.; Jones, A. D.; O'Hare, M.; Kammen, D. M. *Science* **2006**, *311*, 506−508.
(11) Hill, J.; Nelson, E.; Tilman, D.; Polasky, S.; Tiffany, D. *Proc. Natl. Acad. Sci. U.S.A.* **2006**, *103*, 11206−11210.
(12) Kniel, L.; Winter, O.; Stork, K. *Ethylene: Keystone to the Petrochemical Industry*; Marcel Dekker: New York, 1980.
(13) Mills, G. A.; Ecklund, E. E. *Annu. Rev. Energy* **1987**, *12*, 47−80.
(14) Hori, Y. In *Modern Aspects of Electrochemistry*; Vayenas, C., White, R., Gamboa-Aldeco, M., Eds.; Springer: New York, 2008; pp 89−189.
(15) Qiao, J.; Liu, Y.; Hong, F.; Zhang, J. *Chem. Soc. Rev.* **2014**, *43*, 631−675.
(16) Montoya, J. H.; Peterson, A. A.; Nørskov, J. K. *ChemCatChem* **2013**, *5*, 737−742.
(17) Hori, Y.; Murata, A.; Takahashi, R. *J. Chem. Soc., Faraday Trans. 1* **1989**, *85*, 2309−2326.
(18) Kuhl, K. P.; Cave, E. R.; Abram, D. N.; Jaramillo, T. F. *Energy Environ. Sci.* **2012**, *5*, 7050−7059.
(19) Tang, W.; Peterson, A. A.; Varela, A. S.; Jovanov, Z. P.; Bech, L.; Durand, W. J.; Dahl, S.; Nørskov, J. K.; Chorkendorff, I. *Phys. Chem. Chem. Phys.* **2012**, *14*, 76−81.
(20) Bugayong, J.; Griffin, G. L. *Mater. Res. Soc. Symp. Proc.* **2013**, *1542*, 05−11.
(21) Kas, R.; Kortlever, R.; Milbrat, A.; Koper, M. T. M.; Mul, G.; Baltrusaitis, J. *Phys. Chem. Chem. Phys.* **2014**, *16*, 12194−12201.
(22) Hori, Y.; Takahashi, I.; Koga, O.; Hoshi, N. *J. Phys. Chem. B* **2002**, *106*, 15−17.
(23) Yano, H.; Tanaka, T.; Nakayama, M.; Ogura, K. *J. Electroanal. Chem.* **2004**, *565*, 287−293.
(24) Li, C. W.; Ciston, J.; Kanan, M. W. *Nature* **2014**, *508*, 504−507.
(25) Reske, R.; Duca, M.; Oezaslan, M.; Schouten, K. J. P.; Koper, M. T. M.; Strasser, P. *J. Phys. Chem. Lett.* **2013**, *4*, 2410−2413.
(26) Chen, C. S.; Handoko, A. D.; Wan, J. H.; Ma, L.; Ren, D.; Yeo, B. S. *Catal. Sci. Technol.* **2015**, *5*, 161−168.
(27) Hori, Y.; Takahashi, I.; Koga, O.; Hoshi, N. *J. Mol. Catal. A: Chem.* **2003**, *199*, 39−47.
(28) Kim, D.; Lee, S.; Ocon, J. D.; Jeong, B.; Lee, J. K.; Lee, J. *Phys. Chem. Chem. Phys.* **2015**, *17*, 824−830.
(29) Yano, J.; Yamasaki, S. *J. Appl. Electrochem.* **2008**, *38*, 1721−1726.
(30) Li, C. W.; Kanan, M. W. *J. Am. Chem. Soc.* **2012**, *134*, 7231−7234.
(31) Kas, R.; Kortlever, R.; Yılmaz, H.; Koper, M. T. M.; Mul, G. *ChemElectroChem* **2015**, *2*, 354−358.
(32) Hori, Y.; Takahashi, R.; Yoshinami, Y.; Murata, A. *J. Phys. Chem. B* **1997**, *101*, 7075−7081.
(33) Mukhopadhyay, A. K.; Chakraborty, A. K.; Chatterjee, A. P.; Lahiri, S. K. *Thin Solid Films* **1992**, *209*, 92−96.
(34) Yeo, B. S.; Klaus, S. L.; Ross, P. N.; Mathies, R. A.; Bell, A. T. *ChemPhysChem* **2010**, *11*, 1854−1857.
(35) Le, M.; Ren, M.; Zhang, Z.; Sprunger, P. T.; Kurtz, R. L.; Flake, J. C. *J. Electrochem. Soc.* **2011**, *158*, E45−E49.
(36) Bonvalot-Dubois, B.; Dhalenne, G.; Berthon, J.; Revcolevschi, A.; Rapp, R. A. *J. Am. Ceram. Soc.* **1988**, *71*, 296−301.
(37) Niaura, G. *Electrochim. Acta* **2000**, *45*, 3507−3519.
(38) Beverskog, B.; Puigdomenech, I. *J. Electrochem. Soc.* **1997**, *144*, 3476−3483.
(39) Takahashi, I.; Koga, O.; Hoshi, N.; Hori, Y. *J. Electroanal. Chem.* **2002**, *533*, 135−143.
(40) Calle-Vallejo, F.; Koper, M. T. M. *Angew. Chem., Int. Ed.* **2013**, *52*, 7282−7285.
(41) Hatsukade, T.; Kuhl, K. P.; Cave, E. R.; Abram, D. N.; Jaramillo, T. F. *Phys. Chem. Chem. Phys.* **2014**, *16*, 13814−13819.
(42) Schouten, K.; Kwon, Y.; Van der Ham, C.; Qin, Z.; Koper, M. *Chem. Sci.* **2011**, *2*, 1902−1909.
(43) Vollmer, S.; Witte, G.; Wöll, C. *Catal. Lett.* **2001**, *77*, 97−101.
(44) Greeley, J.; Jaramillo, T. F.; Bonde, J.; Chorkendorff, I.; Norskov, J. K. *Nat. Mater.* **2006**, *5*, 909−913.
(45) Zhang, Y.-J.; Sethuraman, V.; Michalsky, R.; Peterson, A. A. *ACS Catal.* **2014**, *4*, 3742−3748.
(46) Wu, J.; Risalvato, F. G.; Ma, S.; Zhou, X.-D. *J. Mater. Chem. A* **2014**, *2*, 1647−1651.

DOI: 10.1021/cs502128q
ACS Catal. 2015, 5, 2814−2821